Journal of Rock Mechanics and Geotechnical Engineering 12 (2020) 1103–1111

Contents lists available at ScienceDirect

Journal of Rock Mechanics and Geotechnical Engineering

journal homepage: www.jrmge.cn

Full Length Article

Pile end bearing capacity in rock mass using cavity expansion theory

Haythem Gharsallaoui*, Mustafa Jafari, Alain Holeyman

Department of Civil and Environmental Engineering (GCE), Institute of Mechanics, Materials and Civil engineering (iMMC), Université Catholique de Louvain (UCLouvain), Louvain-la-Neuve, Belgium

ARTICLE INFO

Article history:
Received 20 August 2019
Received in revised form
26 February 2020
Accepted 18 March 2020
Available online 31 July 2020

Keywords:
Hoek-Brown failure criterion
Spherical cavity
Limit pressure
End bearing capacity

ABSTRACT

Much empiricism is involved in design of rock-socketed piles in rock masses. In light of this, an analytical solution based on the cavity expansion theory is proposed for calculating the ultimate bearing capacity at the tip of a pile embedded in rock masses obeying the Hoek-Brown failure criterion. The ultimate end bearing capacity is evaluated by assuming that the pressure exerted at the boundaries of a pressure bulb immediately beneath the pile tip is equal to the limit pressure required to expand a spherical cavity. In addition, a relationship is derived to predict the pile load-settlement response. To demonstrate the applicability of the presented solution, the results of this study were compared to those of 91 field tests from technical literature. Despite the limitations, it is found that the end bearing resistance computed by the present work is in good agreement with the field test results.

1. Introduction

Piles are commonly-used forms of foundations that provide support for structures, transferring their load to layers of soil or rocks that have enough bearing capacity and suitable settlement characteristics. Nevertheless, assessment of the base resistance of a pile embedded in rock mass is a common issue in civil engineering towards which several empirical approaches have been proposed (Coates, 1965; Rowe and Armitage, 1987; Le Tirant and Marshall, 1992; Zhang and Einstein, 1998; Vipulanandan et al., 2007). Some of these approaches are based on either full-scale in situ tests or laboratory tests. The empirical relationships take the form of a linear/power function of the unconfined compressive strength (UCS) of the intact rock σ_{ci} as

$$q_{b.ult} = \alpha {\sigma_{ci}}^{k} \tag{1}$$

where $q_{b.ult}$ is the ultimate end bearing capacity, and α and k are the bearing capacity coefficients (dimensionless). Table 1 summarizes the values of α and k for some empirical approaches.

To develop these empirical relations, different interpretations of the load test data are used by original authors. According to those interpretations, the ultimate end bearing capacity is defined by way of conventions as:

(1) The bearing resistance at a certain pile head displacement, say 10% of the pile diameter;
(2) The bearing resistance at a certain pile base displacement, say 5% of the pile diameter; and
(3) The maximum applied test load.

Moreover, the ultimate end bearing capacity can be deduced by using either the finite element method or the hyperbolic load transfer function approach to analyze the load-displacement response of the rock-socketed piles. Indeed, the measured load-displacement curve can be matched and subsequently the ultimate end bearing capacity can be determined at a certain pile base or head settlement of 5% or 10%. Because of these different interpretations, it is hard to figure out which one gives accurate estimations of ultimate limit state (ULS). Besides, the “so-called” ultimate end bearing capacity determined from Eq. (1) is not necessarily the ‘true’ ultimate one.

On the other hand, these empirical relations have limitations related to using only the UCS of the intact rock σ_{ci} to predict the end bearing capacity. σ_{ci} is only one of many other parameters that affect the strength of the rock mass. With that in mind, Zhang (2010) developed a new relation for determining $q_{b.ult}$ by considering the effect of discontinuities, represented by the rock quality designation (RQD), on σ_{ci}. Still, his empirical relation has limitation related to using only RQD to represent the effect of discontinuities.

* Corresponding author.
E-mail address: haythem.gharsallaoui@uclouvain.be (H. Gharsallaoui).
Peer review under responsibility of Institute of Rock and Soil Mechanics, Chinese Academy of Sciences.

https://doi.org/10.1016/j.jrmge.2020.03.004

Table 1
End bearing capacity coefficients for some empirical approaches.

Source	α	k
Coates (1965)	3	1
Rowe and Armitage (1987)	2.7	1
Le Tirant and Marshall (1992)	4.5	1
Zhang and Einstein (1998)	4.83	0.51
Vipulanandan et al. (2007)	4.66	0.56

Many other factors of the rock mass rating (RMR) system such as spacing, condition and orientation of discontinuities have a significant effect on the strength of the rock mass. In light of this, rock masses can be better characterized by the Hoek-Brown (H–B) failure criterion (Hoek et al., 2002), which allows for rock structure and surface conditions using the geological strength index (GSI). Kulhawy and Prakoso (1999) stated that practicing engineers should use GSI as an alternative to the RQD in order to prescribe the rock surface state. As a result, this failure criterion has often been used in the literature to provide analytical solutions. The analytical methods for computing the end bearing capacity of piles are mostly based on two general approaches: the method of characteristic lines and the cavity expansion method.

Using the characteristic lines method, Serrano and Olalla (2002) developed an analytical method for computing the bearing capacity at the tip of a pile embedded in a rock mass that obeys the 1997 version of the H–B failure criterion (Hoek and Brown, 1997). Their solution was later generalized for the 2002 version (Hoek et al., 2002). Their derivation is based on the analyses of a wall in plane strain conditions. By adopting an associated flow rule, they used the characteristic lines method generalized for nonlinear failure criterion to analyze the plastic zone. The major shortcoming of their method is that the rock mass is hypothesized as rigid-plastic. Hence, the bearing capacity does not depend on the elastic parameters of the rock mass. Besides, results gained from their theory, when compared to in situ test results (Serrano et al., 2014), showed a high scatter and did not yield satisfactory results which put in doubt their methodology and its applicability to such problem.

In this paper, an analytical solution of pile end bearing capacity is proposed by employing the cavity expansion method. In this approach, the pile is assumed to be sufficiently embedded such that surface effect is neglected. It is further assumed that the pressure exerted at the boundaries of the pressure bulb of rock immediately beneath the pile tip is equal to the limit pressure required to expand a spherical cavity. Then the problem of pile end bearing capacity reduces to determination of the limit pressure. To this end, Gharsallaoui et al. (2019, 2020) developed an original relationship between cavity expansion and pressure exerted to the cavity wall for both perfectly plastic and brittle plastic H–B post failure. Besides, an analytical solution of the limit pressure was proposed by considering the problem of both cylindrical and spherical cavity expansions in an infinite elasto-perfectly plastic H–B material, and by adopting the large strain theory (Gharsallaoui et al., 2020). Therefore, a solution for pile end bearing capacity problem will be proposed based on the aforementioned analytical solutions of the limit pressure.

This paper is organized as follows. A brief recall of the generalized H–B failure criterion and its scaled form is provided in Section 2. Description of the considered problem is detailed in Section 3. Basic hypothesis for computing the limit pressure required to expand a spherical cavity and the expression of the analytical solution of the limit pressure are summarized in Section 4. Section 5 describes two failure mechanisms implemented for the estimates of the ultimate end bearing capacity. Finally, a comparison with state of the art is given in Section 6.

2. Hoek-Brown material behavior

The H–B failure criterion was first introduced in 1980 with its latest update in the 2018 edition (Hoek and Brown, 2019). It is defined as (positive compressive stresses):

$$\sigma_1' = \sigma_3' + \sigma_{\mathrm{ci}}\left(m_{\mathrm{b}}\frac{\sigma_3'}{\sigma_{\mathrm{ci}}} + s\right)^a \tag{2}$$

where σ_1' and σ_3' denote, respectively, the major and minor principal stresses at failure under triaxial loading conditions; and the strength parameters m_{b}, s and a describe the rock mass strength characteristics and they depend on the GSI, the disturbance factor D and the intact frictional strength parameter m_{i}. A detailed description of the criterion can be found elsewhere (Hoek et al., 2002).

It should be emphasized that the above failure criterion expression can be simplified and scaled as formulated by Gharsallaoui et al. (2019, 2020), to give the following form:

$$\sigma_1^* = \sigma_3^* + {\sigma_3^*}^a \tag{3}$$

where σ_1^* and σ_3^* are the scaled (reflected by an asterisk as superscript) major and minor principal stresses, respectively. Scaled stresses are defined naturally as

$$\sigma_j^* = \frac{\sigma_j'}{\sigma_{\mathrm{ci}} m_{\mathrm{b}}^{\beta}} + \frac{s}{m_{\mathrm{b}}^{\beta/a}} \quad (j = 1 \text{ and } 3) \tag{4}$$

where β is a constant solely depending on the exponent $a \neq 1$, and $\beta = a/(1-a)$.

On the other hand, normal and shear stresses are related to principal stresses by the following equations (Balmer, 1952):

$$\sigma_{\mathrm{n}}' = \frac{\sigma_1' + \sigma_3'}{2} - \frac{\sigma_1' - \sigma_3'}{2}\,\frac{\mathrm{d}\sigma_1'/\mathrm{d}\sigma_3' - 1}{\mathrm{d}\sigma_1'/\mathrm{d}\sigma_3' + 1} \tag{5}$$

$$\tau = (\sigma_1' - \sigma_3')\,\frac{\sqrt{\mathrm{d}\sigma_1'/\mathrm{d}\sigma_3'}}{\mathrm{d}\sigma_1'/\mathrm{d}\sigma_3' + 1} \tag{6}$$

where σ_{n}' is the normal stress; τ is the shear stress; and $\mathrm{d}\sigma_1'/\mathrm{d}\sigma_3' = 1 + a m_{\mathrm{b}}\left(m_{\mathrm{b}}\frac{\sigma_3'}{\sigma_{\mathrm{ci}}} + s\right)^{a-1}$ is obtained by direct derivation of Eq. (2).

With the same manipulations, normal and shear stresses can be scaled. It is found that their expressions are related to each other in a parametric form depending exclusively on the scaled minor principal stress σ_3^*:

$$\sigma_{\mathrm{n}}^* = \frac{\sigma_{\mathrm{n}}'}{\sigma_{\mathrm{ci}} m_{\mathrm{b}}^{\beta}} + \frac{s}{m_{\mathrm{b}}^{\beta/a}} = \sigma_3^* + \frac{{\sigma_3^*}^a}{\mathrm{d}\sigma_1^*/\mathrm{d}\sigma_3^* + 1} \tag{7}$$

$$\tau^* = \frac{\tau}{\sigma_{\mathrm{ci}} m_{\mathrm{b}}^{\beta}} = (\sigma_{\mathrm{n}}^* - \sigma_3^*)\sqrt{\mathrm{d}\sigma_1^*/\mathrm{d}\sigma_3^*} = {\sigma_3^*}^a \frac{\sqrt{\mathrm{d}\sigma_1^*/\mathrm{d}\sigma_3^*}}{\mathrm{d}\sigma_1^*/\mathrm{d}\sigma_3^* + 1} \tag{8}$$

where $\mathrm{d}\sigma_1^*/\mathrm{d}\sigma_3^* = 1 + a{\sigma_3^*}^{a-1}$ is obtained by direct derivation of Eq. (3).

Use of Eqs. (7) and (8) rather than Eqs. (5) and (6) leads to important simplification in the analysis of stresses in rock mass. This will be detailed in Section 5, when considering the problem of

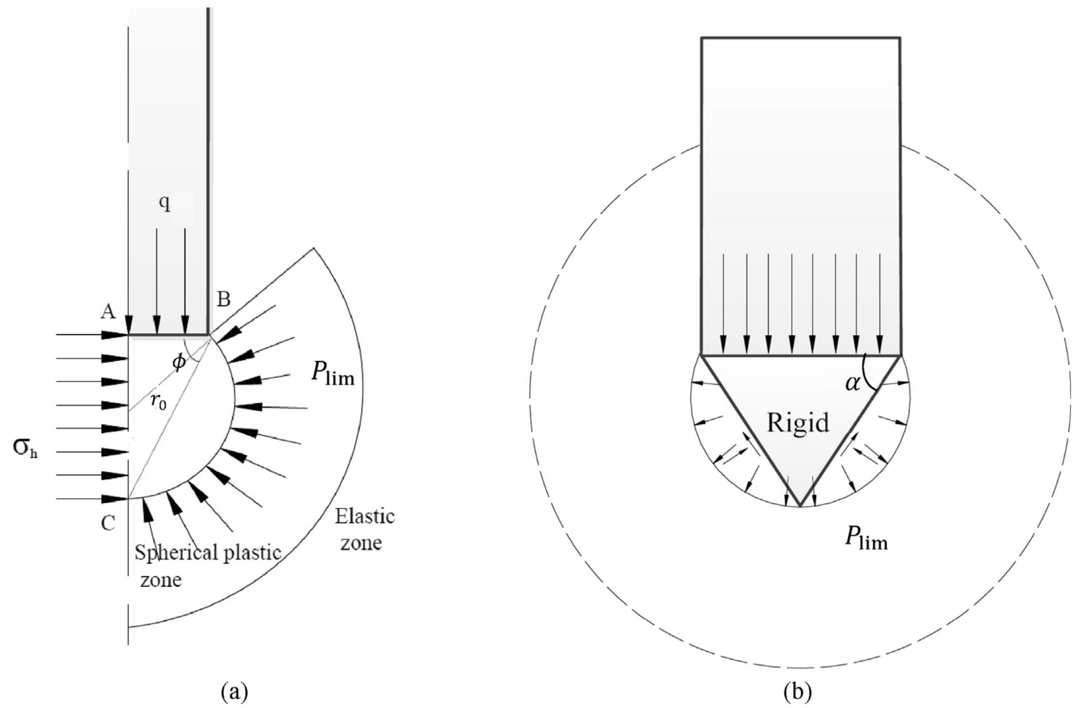

Fig. 1. Sketches of failure mechanisms around the pile tip: (a) Yasufuku and Hyde (1995), and (b) Vesic (1973).

the ultimate end bearing capacity of a pile embedded in H–B material.

3. Problem statement

An important assumption in the use of cavity expansion theory in the context of pile end bearing capacity is that the pressure exerted at the boundaries of the plastic bulb immediately beneath the pile tip is equal to the limit pressure P_{lim} required to expand a spherical cavity. Then, the ultimate end bearing capacity $q_{b.ult}$ can be related to the limit pressure based on two modes.

The failure mechanism of mode 1, which was initially postulated by Yasufuku and Hyde (1995) for crushable sand, is illustrated in Fig. 1. In this mode, active earth pressure conditions are considered to exist immediately beneath the pile tip and moment equilibrium is considered about point *B*. The ultimate bearing capacity of this mode can be found as a function of the friction angle ϕ of the soil as

$$(q_{b.ult})_1 = \frac{P_{lim}}{1 - \sin\phi} \tag{9}$$

The failure mechanism of mode 2 is also illustrated in Fig. 1 (Vesic, 1973). This method assumes a rigid cone of soil beneath the pile tip, with an angle $\alpha = \pi/4 + \phi/2$. Outside the conical region, it is assumed that the normal stress acting on the cone face is equal to the limit pressure P_{lim}. A relationship between $(q_{b.ult})_2$ and P_{lim} can be obtained considering vertical equilibrium, i.e.

$$(q_{b.ult})_2 = P_{lim} + \tau\tan\alpha \tag{10}$$

where the shear stress τ is given as per Eq. (6).

It should be emphasized that unlike the model proposed by Yasufuku and Hyde (1995), the Vesic (1973)'s model takes into account both cohesion and friction angle of the soil. Given that an H–B material is characterized by an instantaneous cohesion and an instantaneous friction angle (depending on the confining stress), the Vesic (1973)'s model is considered to be more reasonable to describe the failure mechanism of pile embedded in H–B material. A comparison between results gained from these two modes is detailed in Section 5.

For both modes, all that remains is to provide how the limit pressure of a spherical cavity is calculated for a material obeying the nonlinear H–B failure criterion. This will be summarized in the following section.

4. Limit pressure for expanding spherical cavity

In this section, we evaluated the limit pressure required to expand a spherical cavity in H–B material. Details of how the expression of the limit pressure was derived could be found in Gharsallaoui et al. (2020). Only basic hypothesis and main results are presented hereinafter.

4.1. Basic hypothesis

A spherical cavity expansion in an infinite elasto-perfectly plastic H–B material is considered. The geometry of the problem and the boundary conditions are depicted in Fig. 2. Let r_i be the internal radius of the cavity and P_0 the far field radial pressure. Let P_i be the internal pressure applied on cavity wall that increases monotonically from its initial value P_0. As the internal pressure P_i increases, the rock mass will initially behave in an elastic manner, until reaching a yield pressure P_{yield}. When the internal pressure P_i exceeds P_{yield}, a plastic region will start spreading from r_i to the "plastic" radius r_p. The remainder of the domain ($r \geq r_p$) belongs to the elastic region.

Note that the major and minor principal stresses are assumed to be equal to the radial and circumferential stresses, respectively, i.e. $\sigma_1 = \sigma_r$ and $\sigma_3 = \sigma_\theta$.

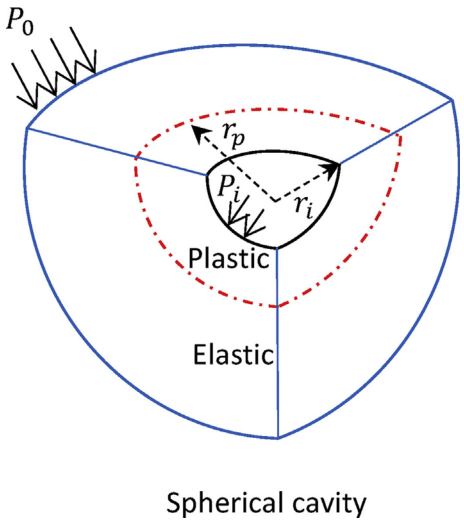

Fig. 2. Geometry of the problem and boundary conditions.

4.2. Limit pressure

By adopting the large strain theory, Gharsallaoui et al. (2020) demonstrated that cavity expansion and pressure exerted to the cavity wall are related to each other by the following implicit relationship:

$$\left(\frac{r_{\mathrm{i}}}{r_{\mathrm{i0}}}\right)^{2\omega+1} = \frac{\Omega^{2\omega+1}}{(1-\delta)^{2\omega+1} - \frac{1}{\eta}\int_{R_{\mathrm{p}}}^{R_{\mathrm{i}}} \frac{D_1[aW_0(\rho)]^{\frac{\beta}{a}} + D_2[aW_0(\rho)]^{\beta}}{\rho^{\frac{\beta(2\omega+1)}{2}+1}}\mathrm{d}\rho} \tag{11}$$

where r_{i0} is the original cavity radius before cavity expansion starts; Ω is the inverse of the normalized plastic radius defined by $\Omega = r_{\mathrm{i}}/r_{\mathrm{p}} = (R_{\mathrm{p}}/R_{\mathrm{i}})^{\beta/k}$; ω is the dilatancy coefficient computed by $\omega = (1-\sin\psi)/(1+\sin\psi)$ with ψ as the dilatancy angle; and D_1, D_2 and η are the dimensionless coefficients defined as

$$\left.\begin{aligned} D_1 &= \frac{(1+2\omega)(1-2\nu)}{2I_{\mathrm{r}}(1+\nu)} \\ D_2 &= \frac{1-2\nu\omega}{2I_{\mathrm{r}}(1+\nu)} \\ \eta &= \frac{\mathrm{e}^{D_1 P_0^*}\left(\beta\dfrac{2\omega+1}{2}\right)^{-1}}{R_{\mathrm{p}}^{\beta\frac{2\omega+1}{2}}} \end{aligned}\right\} \tag{12}$$

The parameter δ in Eq. (11) is the normalized displacement at the elasto-plastic boundary, which is expressed as a function of the rigidity index and the scaled far field and yields pressures as

$$\delta = \frac{1}{4I_{\mathrm{r}}}\left(P_{\mathrm{y}}^* - P_0^*\right) \tag{13a}$$

where

$$I_{\mathrm{r}} = \frac{G}{\sigma_{\mathrm{ci}}\, m_{\mathrm{b}}^{\beta}} \tag{13b}$$

The parameters R_{p} and R_{i} in Eq. (11) are the lower and upper integration limits, respectively. They are defined as solutions of the following equations:

$$P_{\mathrm{y}}^* = [aW_0(R_{\mathrm{p}})]^{\beta/a} + [aW_0(R_{\mathrm{p}})]^{\beta} \tag{14}$$

$$P_{\mathrm{i}}^* = [aW_0(R_{\mathrm{i}})]^{\beta/a} + [aW_0(R_{\mathrm{i}})]^{\beta} \tag{15}$$

The parameter W_0 in Eq. (11) is the 0th branch of the Lambert function (Omega function). Note that the scaled yield pressure P_{y}^* should be computed from the following expression:

$$\left(P_{\mathrm{y}}^* - P_0^*\right) = -\frac{1}{2}\left(P_{\mathrm{y}}^* - P_0^*\right) + \left[P_0^* - \frac{1}{2}\left(P_{\mathrm{y}}^* - P_0^*\right)\right]^a \tag{16}$$

The above equation provides an explicit solution when $a = 0.5$ as

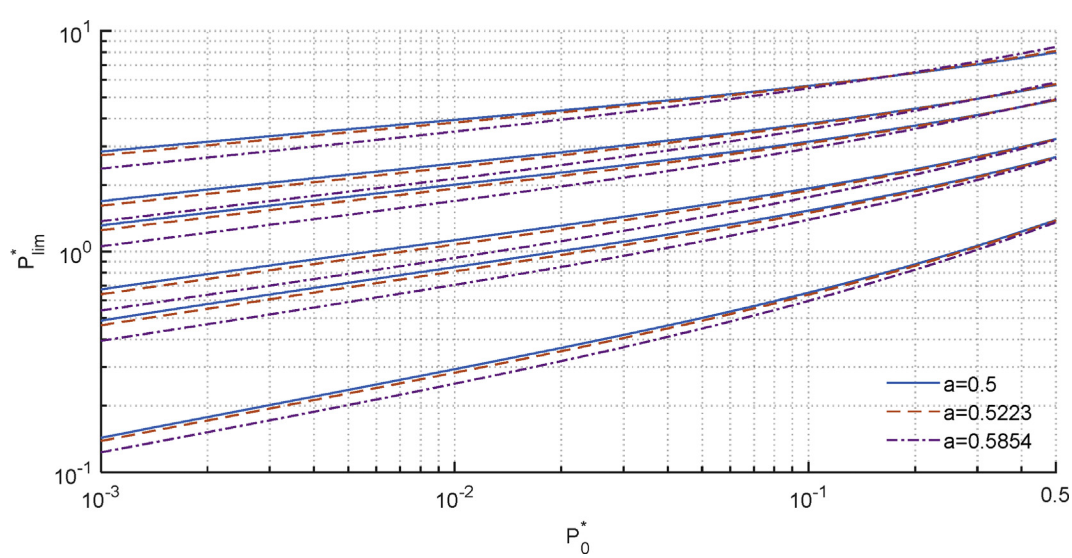

Fig. 3. Limit pressure chart by setting $\psi = 0°$ and $\nu = 0.25$ (after Gharsallaoui et al., 2020). Values of $I_{\mathrm{r}}^{-1} = 10^{-3}$, 5×10^{-3}, 10^{-2}, 5×10^{-2}, 10^{-1}, and 1 correspond to the groups of curves from top to bottom.

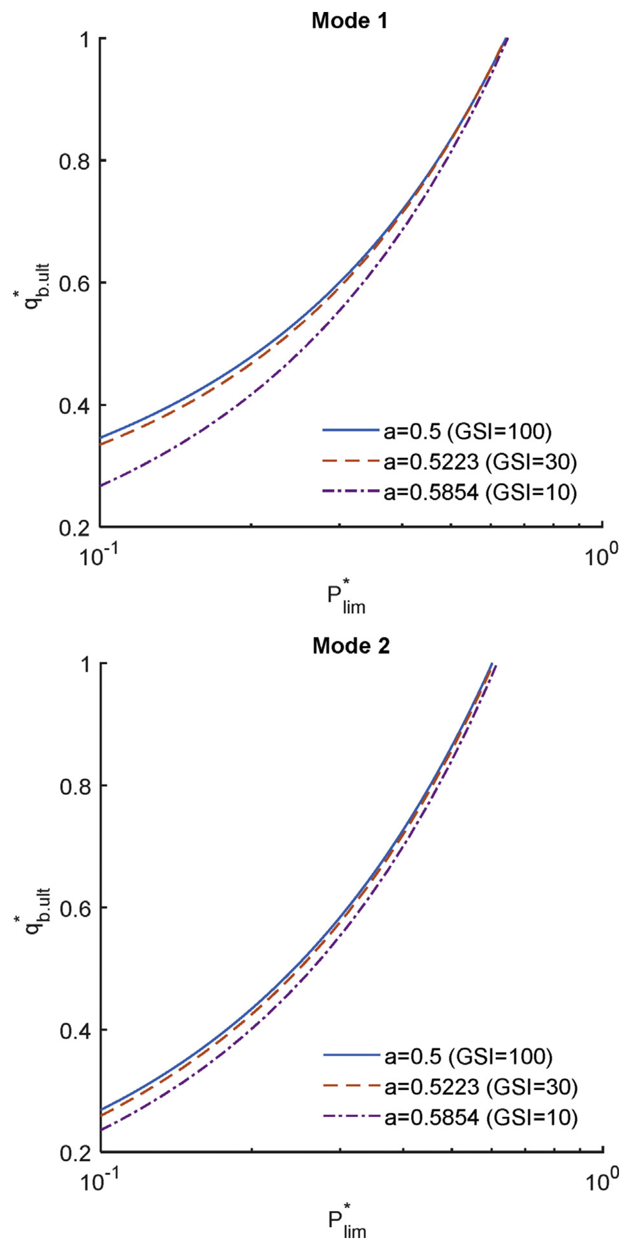

Fig. 4. 'True' ultimate bearing capacity for failure mechanisms of modes 1 and 2.

$$P^*_{y\,|a=0.5} = P^*_0 + \frac{\sqrt{36P^*_0+1}-1}{9} \tag{17}$$

When $a \neq 0.5$, there is no explicit solution and Eq. (16) should be solved numerically. On the other hand, the scaled limit pressure P^*_{lim} can be found by putting $r_i/r_{i0} \to +\infty$ in Eq. (11), i.e.

$$\eta(1-\delta)^{2\omega+1} - \int_{R_p}^{R_i} \frac{e^{D_1[aW_0(\rho)]^{\frac{\beta}{a}}+D_2[aW_0(\rho)]^{\beta}}}{\rho^{\frac{\beta(2\omega+1)}{2}+1}}\,d\rho = 0 \tag{18}$$

It can be noted from Eqs. (11)–(18) that P^*_{lim} depends on five main parameters, which are the far field pressure P^*_0, the rigidity index I_r, the Poisson's ratio ν, the dilatancy angle ψ and the exponent a (i.e. GSI).

A closed-form solution of the limit pressure can be provided by assuming an intact ($a = 0.5$), incompressible ($\nu = 0.5$) H–B material with no plastic volume change ($\psi = 0°$):

$$P^*_{lim} = \left[\frac{W_0(C_1)}{2}\right]^2 + \frac{W_0(C_1)}{2} \tag{19a}$$

where

$$C_1 = \frac{\left(\sqrt{4P^*_{y\,|a=0.5}+1}-1\right)e^{\sqrt{4P^*_{y\,|a=0.5}+1}-1}}{\left[1-(1-\delta)^3\right]^{\frac{2}{3}}} \tag{19b}$$

A chart allowing easy and accurate estimation of the limit pressure is depicted in Fig. 3. The chart is created for $\psi = 0°$. This value leads to conservative estimations of the limit pressure. Indeed, Manandhar and Yasufuku (2013) stated that no plastic volumetric strain should be assumed when computing P_{lim}, i.e. the dilatancy angle will be considered to be zero for large strain analyses.

5. End bearing capacity

In this section, details of how the ultimate end bearing capacity is calculated are given below firstly for failure mechanism of mode 1 and then for mode 2. For failure mechanism of mode 1, the relationship between $(q_{b.ult})_1$ and P_{lim} is given as per Eq. (9). Knowing that the friction angle ϕ is determined from the slope of the tangent to the H–B failure envelope as

$$\frac{d\sigma^*_r}{d\sigma^*_\theta} = \tan^2\left(\frac{\pi}{4}+\frac{\phi}{2}\right) = 1 + a\sigma^{*\,a-1}_\theta \tag{20}$$

By substituting the above expression into Eq. (9) and after some derivations, it is demonstrated that the scaled ultimate end bearing capacity $(q^*_{b.ult})_1$ and the scaled limit pressure P^*_{lim} are related to each other using a parametric form depending exclusively on the scaled circumferential stress σ^*_θ as follows:

Table 2
Rock mass properties and computed end bearing resistance q_b for different settlement values.

Input parameters		H–B derived and intermediate parameters		Limit pressure and ultimate end bearing capacity for both modes		Pile end bearing resistance for both modes		
						s_b/B	$(q_b)_1$ (MPa)	$(q_b)_2$ (MPa)
m_i	2	a	0.5	P^*_{lim} as per Eq. (18)	2.86	10%	44.7	49.5
σ_{ci} (MPa)	25	m_b	2	$(q^*_{b.ult})_1$ as per Eq. (21)	3.38	20%	69.5	77
GSI	100	s	1	$(q^*_{b.ult})_2$ as per Eq. (21)	3.71	50%	104.3	115.5
E_i/σ_{ci}	150	β	1			100%	125.1	138.6
E_{rm} (GPa)	3.73	P^*_0	0.255			$+\infty$	156.4	173.2
ν	0.251	I_r	29.8					
P_0 (MPa)	0.25							

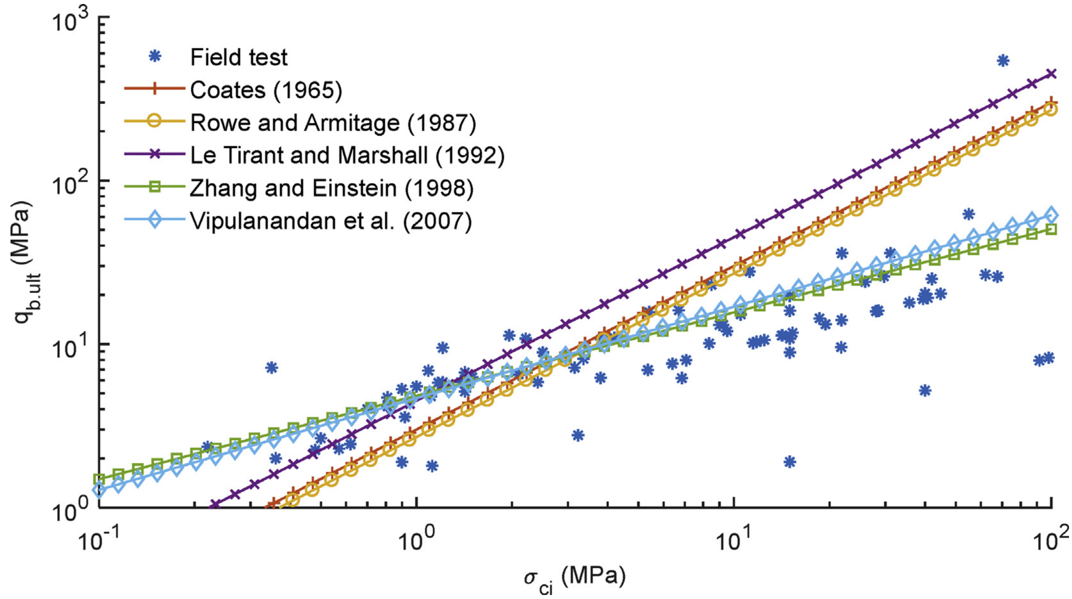

Fig. 5. Ultimate end bearing capacity as a function of the unconfined compressive strength σ_{ci}: Field test vs. empirical relations from Coates (1965), Rowe and Armitage (1987), Le Tirant and Marshall (1992), Zhang and Einstein (1998), and Vipulanandan et al. (2007).

$$\left.\begin{aligned}(q^*_{\mathrm{b.ult}})_1 &= \sigma^*_\theta + \left(1+\frac{a}{2}\right)\sigma^{*a}_\theta + \frac{a}{2}\sigma^{*2a-1}_\theta - \frac{s}{m_\mathrm{b}^{\beta/a}}\frac{a}{2}\sigma^{*a-1}_\theta \\ P^*_{\mathrm{lim}} &= \sigma^*_\theta + \sigma^{*a}_\theta\end{aligned}\right\} \tag{21}$$

For failure mechanism of mode 2, the relationship between $(q_{\mathrm{b.ult}})_2$ and P_{lim} given as per Eq. (10) is further expressed in a scaled form as

$$(q^*_{\mathrm{b.ult}})_2 = P^*_{\mathrm{lim}} + \tau^* \tan\alpha \tag{22a}$$

where

$$\alpha = \frac{\pi}{4} + \frac{\phi}{2} \tag{22b}$$

Subsuming Eqs. (8) and (20) into Eq. (22a) results in following parametric form relating $(q^*_{\mathrm{b.ult}})_2$ and P^*_{lim} by means of σ^*_θ as

$$\left.\begin{aligned}(q^*_{\mathrm{b.ult}})_2 &= \sigma^*_\theta + \sigma^{*a}_\theta \\ P^*_{\mathrm{lim}} &= \sigma^*_\theta + \frac{\sigma^{*a}_\theta}{2 + a\sigma^{*a-1}_\theta}\end{aligned}\right\} \tag{23}$$

The evolutions of both $(q^*_{\mathrm{b.ult}})_1$ and $(q^*_{\mathrm{b.ult}})_2$ as a function of P^*_{lim} are depicted in Fig. 4 for different values of the exponent a (i.e. GSI) and by setting $m_\mathrm{i} = 10$. As can be seen, the ultimate end bearing capacity values derived from both modes are close to each other when $P^*_{\mathrm{lim}} > 0.37$ whereas mode 2 offers conservative values when $P^*_{\mathrm{lim}} < 0.37$. It is also observed that the ultimate end bearing capacity values are relatively constant when $GSI > 30$.

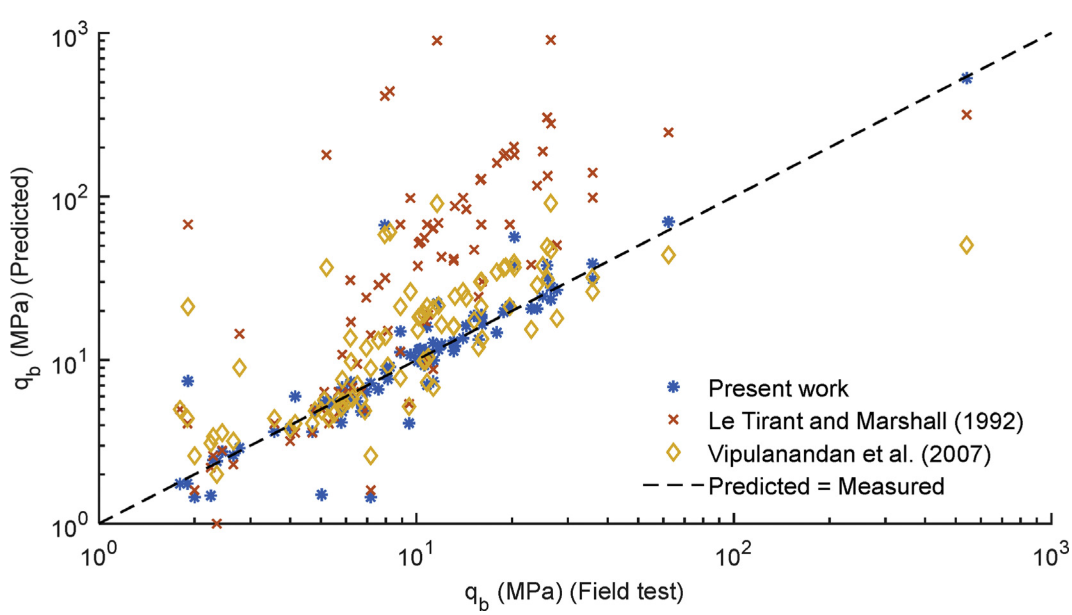

Fig. 6. End bearing resistance: Present work solution vs. empirical approaches from Le Tirant and Marshall (1992) and Vipulanandan et al. (2007).

On the other hand, due to the high capacity of piles in rock masses, it is rarely possible to mobilize the bearing capacity corresponding to the ultimate limit state. As a result, it is important to estimate the end bearing capacity of a pile at a certain settlement level at the pile base in the context of performance-based design. In light of this, it will be necessary to compute the ultimate bearing capacity and the load-settlement behavior of piles. To achieve this, it will be further assumed that the volume of rock mass immediately beneath the pile tip which is displaced due to the pile settlement s_b is equal to the increase of spherical cavity volume, i.e.

$$s_b \frac{\pi B^2}{4} = \frac{4}{3}\pi\left(r_i^3 - r_{i0}^3\right) \tag{24}$$

The instantaneous cavity radius r_i can be expressed as a function of the pile base diameter B as (Yang, 2006):

$$r_i = \frac{B}{2\cos\phi} \tag{25}$$

Therefore, Eq. (24) can be further expressed as

$$\frac{s_b}{B} = \frac{2}{3}\frac{1-\left(\frac{r_{i0}}{r_i}\right)^3}{\cos^3\phi} \tag{26}$$

where r_{i0}/r_i is given as per Eq. (11). Referring to Eq. (20), the term $\cos\phi$ in Eq. (26) can be substituted by the following expression depending exclusively on the circumferential stress $\sigma_\theta^*(R_i)$ as

$$\cos\phi = \frac{2\sqrt{1+a\sigma_\theta^{*a-1}}}{2+a\sigma_\theta^{*a-1}} \tag{27a}$$

where

$$\sigma_\theta^*(R_i) = [aW_0(R_i)]^{\frac{\beta}{a}} \tag{27b}$$

To sum up, the procedure described below should be followed to evaluate the ultimate end bearing capacity ($s_b/B \rightarrow +\infty$) as well as the end bearing resistance for a given settlement s_b/B of a pile embedded in H–B material:

(1) Choose input parameters: m_i, σ_{ci}, D, P_0, G (or E), ν and $\psi = 0°$;
(2) Evaluate H–B derived parameters: a, m_b and s;
(3) Evaluate intermediate parameters: $P_0^* = \frac{P_0}{\sigma_{ci} m_b^\beta} + \frac{s}{m_b^{\beta/a}}$ and $I_r = \frac{G}{\sigma_{ci} m_b^\beta}$;
(4) Evaluate the scaled limit pressure P_{lim}^* as per Eq. (18) or read it approximately from spherical cavity chart (cf. Fig. 3);
(5) Evaluate the scaled ultimate end bearing capacity $q_{b.ult}^*$ for both modes using Eqs. (21) and (23); and
(6) Evaluate the end bearing resistance for a given settlement s_b/B using Eq. (11) combined with Eq. (26) for P_i^*. Then, q_b^* is evaluated as per Eq. (21) for mode 1 and as per Eq. (23) for mode 2.

An example is given below for computing the ultimate end bearing capacity as well as the end bearing resistance of a pile embedded in H–B material with properties similar to that of an undisturbed ($D = 0$) claystone (Hoek, 2006). Table 2 summarizes the rock mass properties and the computed end bearing resistance q_b for different settlement values.

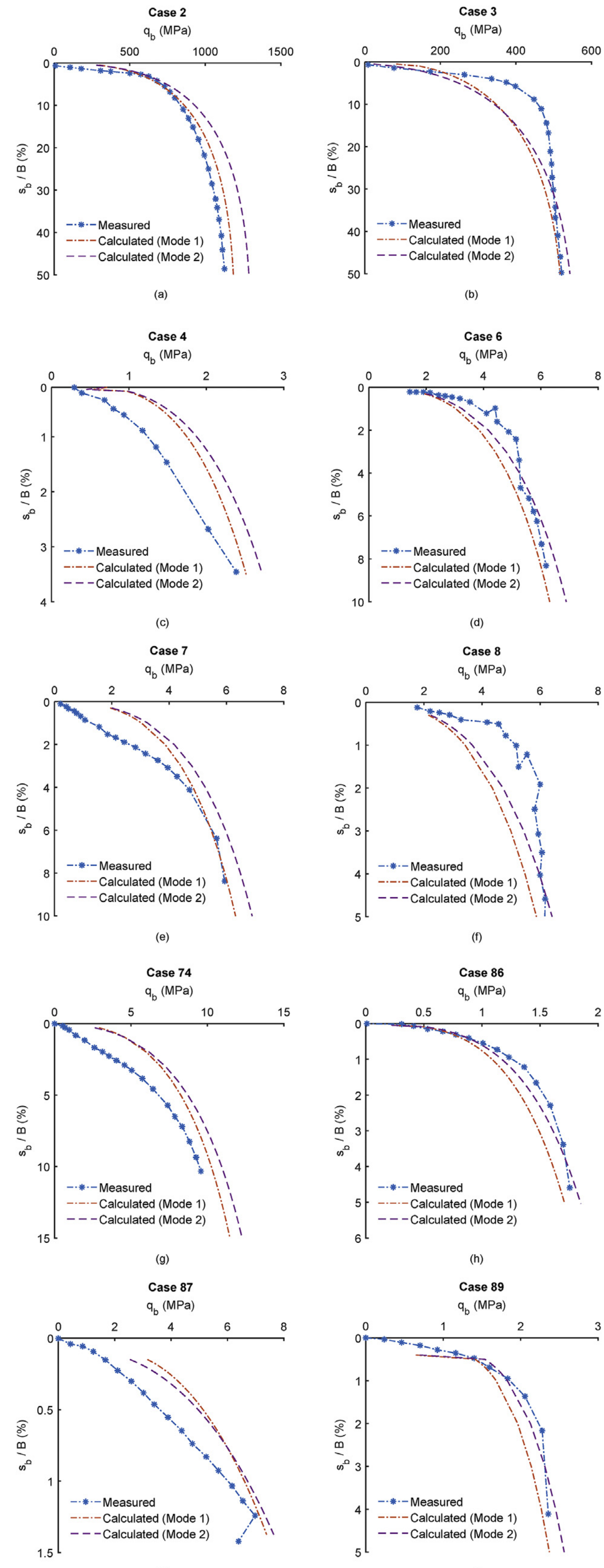

Fig. 7. Load-displacement curves: Present work vs. field test.

6. Comparison with field test results

To demonstrate the applicability of the proposed analytical solution, 91 field tests from the technical literature are summarized in Table A1 in the Appendix. For each case, the rock layer characteristics, measured end bearing resistance and settlements were identified.

It is further assumed that all rocks listed in Table A1 obey the H–B failure criterion. Indeed, these type of rocks were characterized as H–B material and their parameters are published in Hoek (2006).

In order to compute the bearing capacity, the elastic and mechanical properties of the rock mass (deformation modulus E_{rm}, UCS, etc.) were retrieved from the original papers. However, it was still necessary to estimate the parameters of the H–B criterion: GSI, m_i and the elastic modulus for some particular cases. The parameter m_i was estimated based on published guidelines and tables for different rock types (Hoek, 2006). Similarly, the elastic modulus of intact rock was also estimated based on rock type when necessary (Hoek and Diederichs, 2006).

In order to profit from the large amount of test data accumulated using the traditional RMR system, the GSI values can be calculated after Hoek et al. (2013) as

$$GSI = 1.5JCond89 + RQD/2 \tag{28}$$

where $JCond89$ denotes the joint condition rating that varies from 0 to 30. When RQD was not available, the GSI values were estimated based on the rock surface description in the original papers.

Finally, the analytical and measured end bearing resistances are compared in Table A1. The results indicate the crucial role of incorporating the allowable pile settlement in the bearing capacity computations.

A comparison between measured end bearing capacity and those predicted from the empirical relations (Eq. (1)) is depicted in Fig. 5. As can be seen, significant scatter exists. This may be attributed to the fact that these empirical relations rely only on the UCS of the intact rock mass σ_{ci} and do not take into account the rock structure and surface conditions represented by GSI. The measured end bearing resistance is plotted against the computed bearing resistance in Fig. 6. For analytical solution, the mean values of modes 1 and 2 were considered. As can be seen, the present work solution provides better estimations in comparison with the empirical method (Eq. (1)).

To better demonstrate the benefits of the proposed method, the measured load–displacement curve is visualized against the computed curve according to the present work. Fig. 7 displays these curves for cases 2, 3, 4, 6, 7, 8, 74, 86, 87 and 89. As observed, the general trends of the curves agree well.

7. Conclusions

An analytical method for computing the ultimate end bearing capacity $q_{b.ult}$ of a pile embedded in a rock mass that obeys the H–B failure criterion was proposed. This method was developed based on the assumption that the pressure exerted at the boundaries of the bulb of rock immediately beneath the pile tip is equal to the limit pressure P_{lim} required to expand a spherical cavity. To compute the limit pressure, an analytical solution which required a numerical integration over the plastic region was presented. Thereafter, $q_{b.ult}$ was evaluated as a function of P_{lim} by adopting two failure mechanisms around the pile tip. The limit pressure was computed by assuming a no dilatant H–B material ($\psi = 0°$). This assumption was on the conservative side since P_{lim} increased for an increasing ψ value.

Results derived from the present work were compared to field load test results of 91 specific cases. It is found that developed solution agreed well with experimental results.

However, the existing empirical relations for estimating the ultimate end bearing capacity do not give reliable estimates. These empirical relations have limitations related to using only the UCS of the intact rock σ_{ci} to predict the end bearing capacity and this parameter is only one of many other parameters that affect the strength of the rock.

Declaration of competing interest

The authors declare that they have no known competing financial interests or personal relationships that could have appeared to influence the work reported in this paper.

Appendix A. Supplementary data

Supplementary data to this article can be found online at https://doi.org/10.1016/j.jrmge.2020.03.004.

Nomenclature

r_i	Cavity radius
r	Radial coordinate
r_p	Plastic radius
P_i	Internal cavity pressure
P_y	Yield pressure
P_0	Far field pressure
P_{lim}	Limit pressure
q_b	End bearing resistance
$q_{b.ult}$	Ultimate end bearing capacity
GSI	Geological strength index of the rock
RMR	Rock mass rating
m_i	Strength parameter of the intact rock
D	Disturbance factor of the rock
s, a, m_b	Hoek-Brown derived parameters
E_i	Deformation modulus of the intact rock
E_{rm}	Deformation modulus of the rock
G	Shear modulus
I_r	Rigidity index
σ'_1	Major principal stress
σ'_3	Minor principal stress
σ_r	Radial stress assumed equal to σ'_1
σ_θ	Circumferential stress assumed equal to σ'_3
σ_{ci}	Uniaxial compressive stress of the intact rock
σ_h	Active earth pressure
τ	Shear stress
σ'_n	Normal stress
ν	Poisson's ratio
ϕ	Friction angle of the rock mass
ψ	Dilatancy angle of the rock mass
ω	Dilatancy coefficient

References

Balmer G. A general analytical solution for Mohr's envelope. Proceedings of ASTM International 1952;52:1260–71.

Coates DF. Rock mechanics principles. Ottawa, Canada: department of mines and technical surveys. 1965.

Gharsallaoui H, Jafari M, Holeyman A. Cavity expansion analysis in elastic-brittle plastic rock mass. In: Proceedings of the 27th European Young Geotechnical Engineers Conference; 2019.

Gharsallaoui H, Jafari M, Holeyman A. Cavity expansion in rock masses obeying the "Hoek–Brown" failure criterion. Rock Mechanics and Rock Engineering 2020;53:927–41.

Hoek E. Practical rock engineering. https://www.rocscience.com/learning/hoeks-corner/course-notes-books; 2006.

Hoek E, Brown ET. Practical estimates of rock mass strength. International Journal of Rock Mechanics and Mining Sciences 1997;34(8):1165–86.
Hoek E, Brown ET. The Hoek–Brown failure criterion and GSI – 2018 edition. Journal of Rock Mechanics and Geotechnical Engineering 2019;11(3):445–63.
Hoek E, Carranza C, Corkum B. Hoek-brown failure criterion – 2002 edition. In: Proceedings of the NARMS-TAC conference. Toronto: Canada; 2002. p. 267–73.
Hoek E, Carter TG, Diederichs MS. Quantification of the geological strength index chart. In: Proceedings of the 47th US rock mechanics/geomechanics symposium. San Francisco, CA: USA. American Rock Mechanics Association (ARMA); 2013. p. 1757–64.
Hoek E, Diederichs MS. Empirical estimation of rock mass modulus. International Journal of Rock Mechanics and Mining Sciences 2006;43:203–15.
Kulhawy FH, Prakoso WA. End bearing capacity of drilled shafts in rock. Journal of Geotechnical and Geoenvironmental Engineering 1999;125(12):1106–10.
Le Tirant P, Marshall N. Offshore pile design. Paris: Éditions Technip; 1992.
Manandhar S, Yasufuku N. Vertical bearing capacity of tapered piles in sands using cavity expansion theory. Soils and Foundations 2013;53(6):853–67.
Rowe RKK, Armitage HHH. A design method for drilled piers in soft rock. Canadian Geotechnical Journal 1987;24(1):126–42.
Serrano A, Olalla C. Ultimate bearing capacity at the tip of a pile in rock - Part 1: Theory. International Journal of Rock Mechanics and Mining Sciences 2002;39(7):833–46.
Serrano A, Olalla C, Galindo RA. Ultimate bearing capacity at the tip of a pile in rock based on the modified Hoek-Brown criterion. International Journal of Rock Mechanics and Mining Sciences 2014;71(7):83–90.
Vesic AS. On penetration resistance and bearing capacity of piles in sand. In: Proceedings of the 8th international conference on soil mechanics and foundation engineering; 1973.
Vipulanandan C, Hussain A, Usluogulari O. Parametric study of open core-hole on the behavior of drilled shafts socketed in soft rock. In: Contemporary Issues in Deep Foundations. American Society of Civil Engineers (ASCE); 2007. p. 1–10.
Yang J. Influence zone for end bearing of piles in sand. Journal of Geotechnical and Geoenvironmental Engineering 2006;132(9):1229–37.
Yasufuku N, Hyde AFL. Pile end-bearing capacity in crushable sands. Géotechnique 1995;45(4):663–76.
Zhang L, Einstein HH. End bearing capacity of drilled shafts in rock. Journal of Geotechnical and Geoenvironmental Engineering 1998;12:574–85.
Zhang L. Prediction of end-bearing capacity of rock-socketed shafts considering rock quality designation (RQD). Canadian Geotechnical Journal 2010;47(10):1071–84.

Haythem Gharsallaoui graduated as a civil engineer with honors from Ecole National d'Ingénieurs de Tunis (ENIT) in 2015. In the same year, he joined the Université Catholique de Louvain in Belgium where he works as a teaching assistant at the Department of Civil and Environmental Engineering. He is also pursuing his PhD in Geotechnical Engineering with the topic "Bearing capacity of shallow and deep foundations in rock mass: Analytical and experimental investigations".